Supporting Information

Influence of the Substrate on the Bulk Properties of Hybrid Lead Halide Perovskite Films

Esteban Climent-Pascual[a], Bruno Clasen Hames[b], Jorge S. Moreno-Ramírez[c], Angel Luis Álvarez[c], Emilio J. Juarez-Perez[d], Elena Mas-Marza[b], Ivan Mora-Seró[b,], Alicia de Andrés[a,*] and Carmen Coya[c,*]*

[a] Instituto de Ciencia de Materiales de Madrid, Consejo Superior de Investigaciones Científicas, Cantoblanco, Madrid 28049, Spain.

[b] Institute of Advanced Materials (INAM), Universitat Jaume I, 12006 Castelló, Spain.

[c] Escuela Técnica Superior de Ingeniería de Telecomunicación (ETSIT), Universidad Rey Juan Carlos, 28933 Madrid, Spain.

[d] Energy Materials and Surface Sciences Unit, Okinawa Institute of Science and Technology Graduate University (OIST), Okinawa, 904-0495 Japan.

** corresponding authors*

Profilometry

Atomic force microscopy AFM images of the used substrates are in **Figure S1**. Measurements were performed using a commercial equipment and software from Nanotec [1] under ambient conditions. Images have been acquired in tapping mode using commercial silicon tips from Nanosensors (PPPQNCHR, 20–30 nm tip diameter). The measured roughness of the substrates are: 3.2, 15.3, 0.8 and 6.8 nm for bare glass, FTO, PEDOT:PSS and TiO_2 respectively.

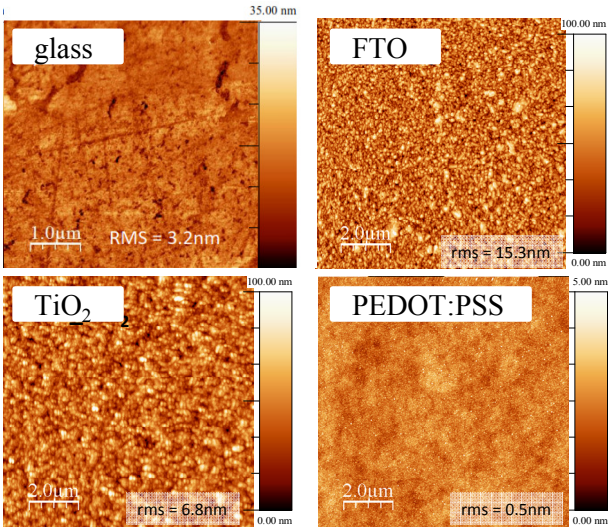

Figure S1. AFM profilometry showing the root mean square (rms) roughness of the four substrates on which the $MAPbCl_xI_{3-x}$ are deposited: (a) glass, (b) FTO, (c) TiO_2 and (d) PEDOT:PSS.

The films thickness of the $MAPbI_{3-x}Cl_x$ films has been evaluated by contact profilometry (Alpha step 200 profilometer, Tenkor Instrument), obtaining around 650, 550, 650 and 750 nm for the thin film growth on glass, glass/FTO/PEDOT:PSS, glass/FTO and glass/FTO/TiO_2 respectively. Profilometry and topography analysis on 500x500 microns area size on each sample and Apex 3D software pack gives us a Root Mean Square Roughness (S_q) of 156, 116, 143 and 126 nm (**Figure S2**, left panel). The different morphologies observed by optical microscopy of $MAPbI_{3-x}Cl_x$ thin films on the four substrates are shown in Figure S2, right panel.

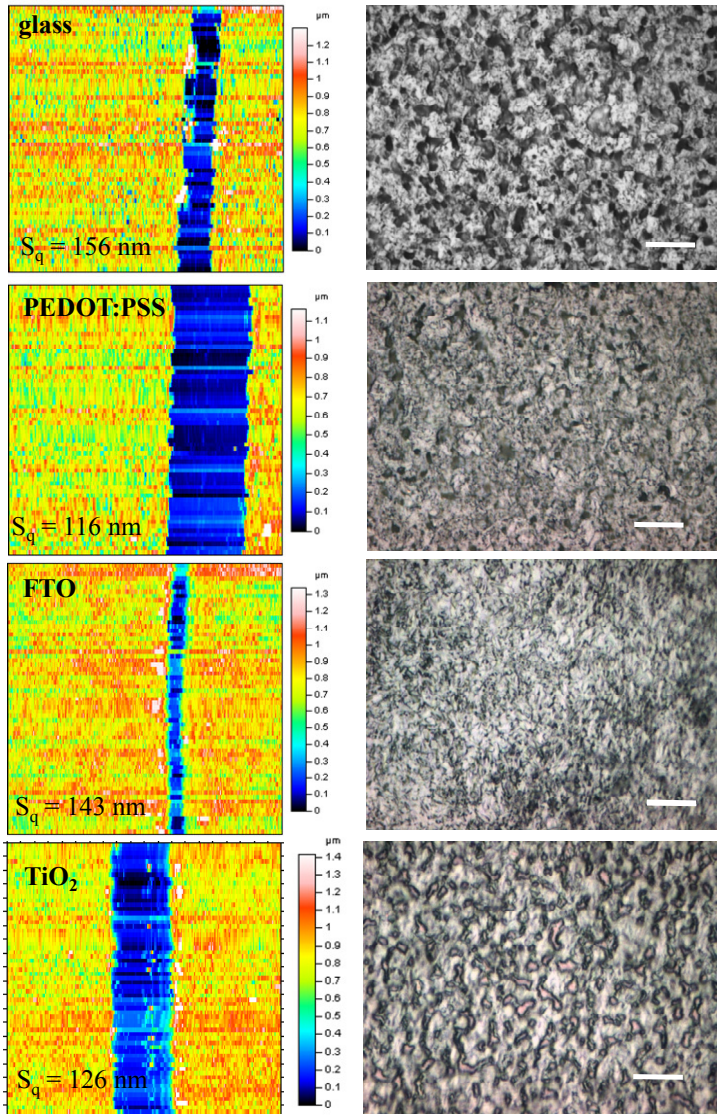

Figure S2. Profilometry and topography analysis (Left panel) on 500x500 μm^2 area size on each sample showing height profile and Root Mean Square Roughness (S_q) for the $MAPbI_{3-x}Cl_x$ thin films on (a) glass, (b) glass/FTO/PEDOT:PSS and (c) glass/FTO and (d) glass/FTO/TiO_2. The images show the groove (blue) made to measure the height step. Right panel: Optical images (73x55 µm) of $CH_3NH_3PbI_{3-x}Cl_x$ thin films growth on (a) glass, (b) glass/FTO/PEDOT:PSS and (c) glass/FTO and (d) glass/FTO/TiO_2. The scale bar is equivalent to 10 µm.

Crystal structure

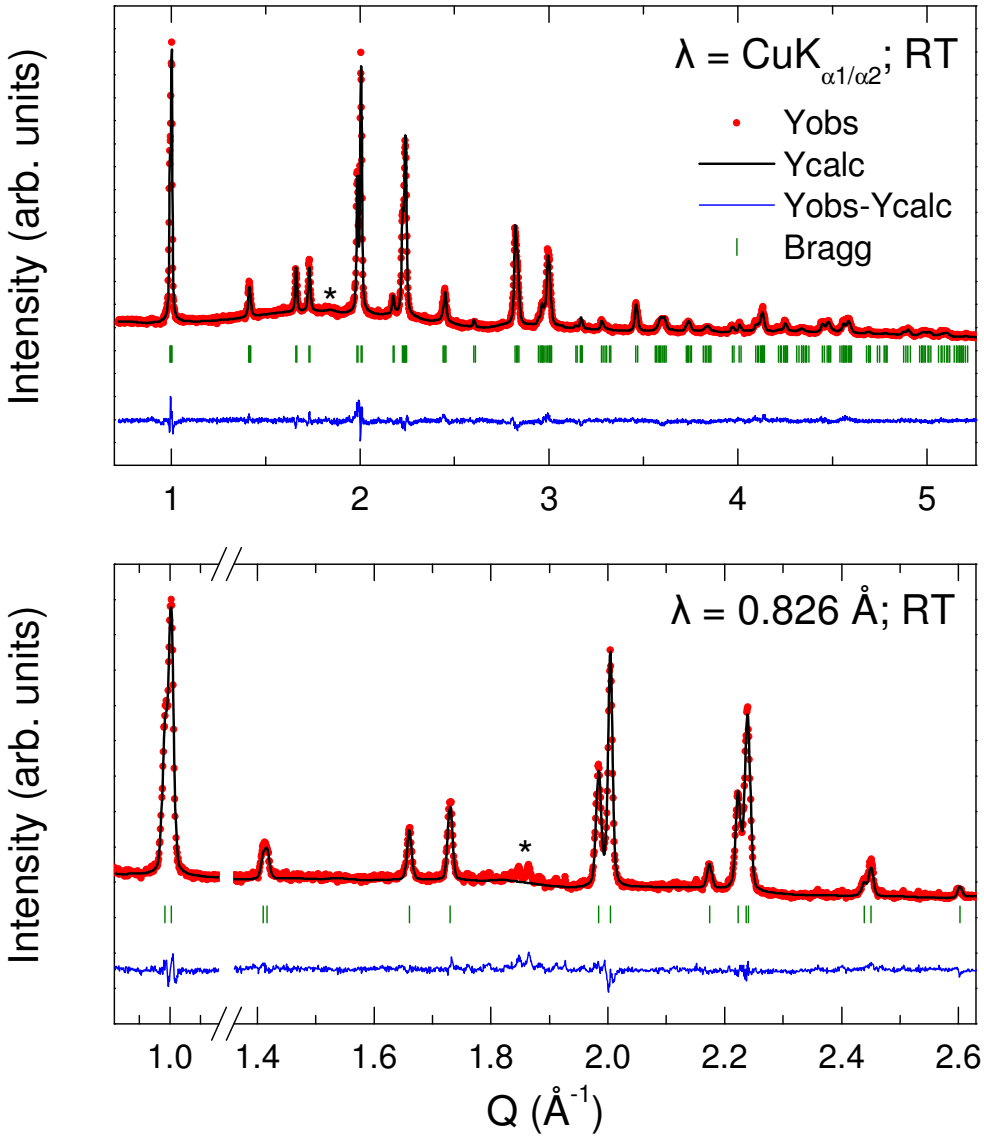

Figure S3. Observed (circles), calculated (solid line) and difference (lower solid line) XRPD (λ = Cu $Kα_1/α_2$) and SXRPD (λ = 0.826 Å) profiles of $MAPbI_3$ powder at RT. Tick marks indicate the position of allowed reflections of $MAPbI_3$ in *I*4*cm* (upper). The asterisk indicates the presence of a minor amount of PbI_2.

In order to refine the crystal structure of the $MAPbI_3$ powder, the non-centrosymmetric *I*4*cm* space group was chosen. These refinements were based on the polar tetragonal structural model previously reported by Stoumpos *et al.* for $MAPbI_3$ single-crystal, where the C−N bonds of the methylammonium cations are fixed parallel to the *c*-axis. [2] The used experimental data were collected on a laboratory diffractometer (D8 Focus,

Bruker; Cu $K_{\alpha 1/\alpha 2}$), and on a six-circle diffractometer (15 KeV; 0.826 Å) at the BM25B (SpLine) beamline at the European Syncrotron facility (ESRF) at RT. The Rietveld plots and the crystallographic data are given in **Figure S3** and **Table S1**, respectively. The C and N atomic positions of the methylammonium cations were not refined taking into account the quality of the collected data.

$CH_3NH_3PbI_3$		*I*4*cm*
a (Å)		8.8695(1)
c (Å)		12.6624(2)
V (Å^3)		996.13(3)
Pb (4*a*)	U_{iso} (Å^2)	0.0386(9)
I_1 (4*a*)	z/c	0.2524(2)
	U_{iso} (Å^2)	0.099(3)
I_2 (8*c*)	x/a	0.2162(3)
	y/b	0.7162(3)
	z/c	0.01249(9)
	U_{iso} (Å^2)	0.0857(16)
C (4*b*)	U_{iso} (Å^2)	0.112(14)
N (4*b*)	U_{iso} (Å^2)	0.112
R_{Bragg} (%)		8.74
R_{wp} (%)		5.63

Table S1. Refined lattice parameters, atomic positions and atomic displacement parameters of $CH_3NH_3PbI_3$ in tetragonal *I*4*cm* (#108) at RT. Agreement factors (R_{Bragg} and R_{wp}) are also given. A minor amount (<4 wt.%) of PbI_2 impurity was found in these samples.

Determination of lattice parameters and preferred orientation degree for the films

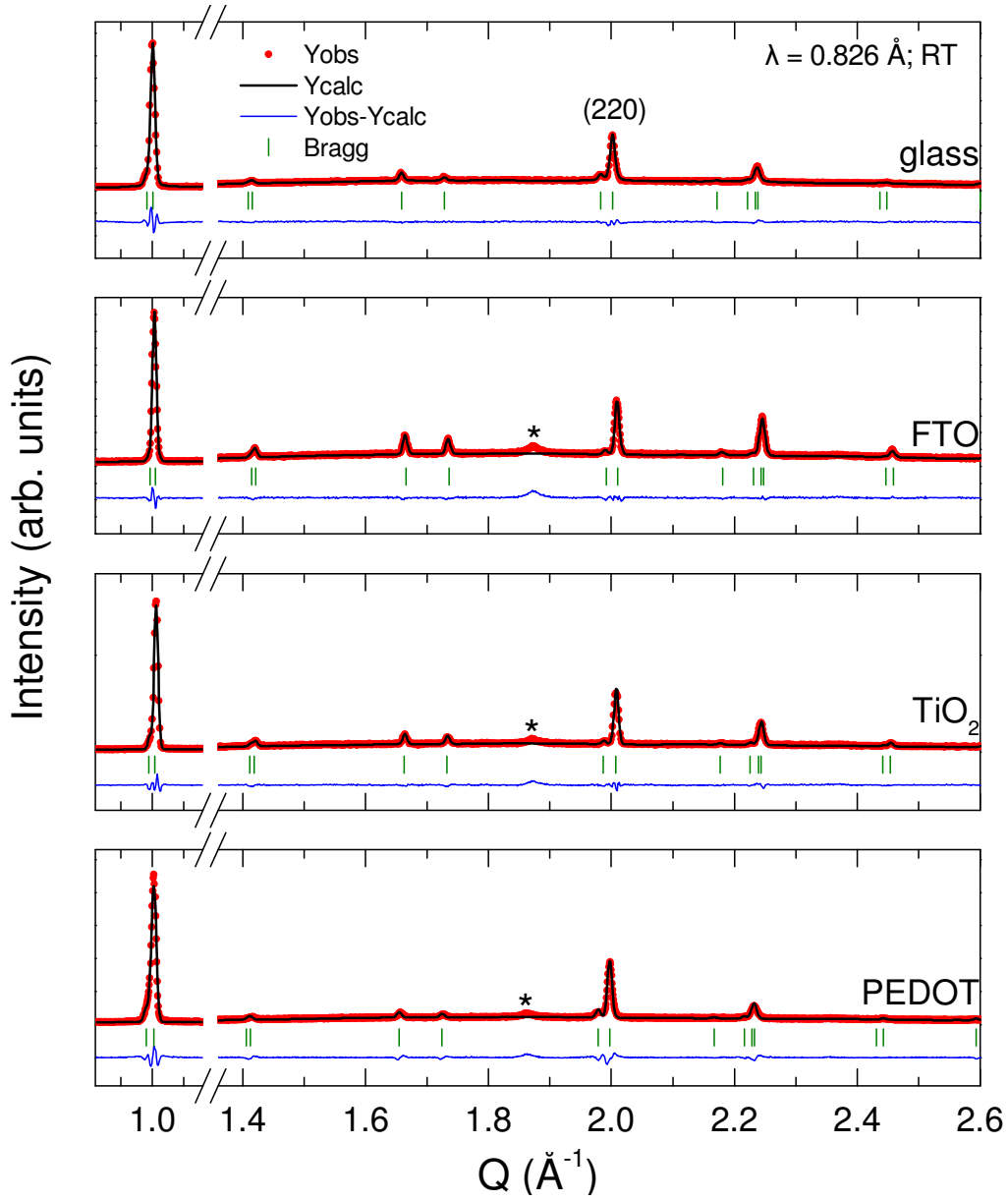

Figure S4. *Le Bail* profile fits (solid line) of SXRPD (λ = 0.826 Å) data (circles) of $MAPbI_3$ films on glass, glass/FTO, glass/FTO/TiO_2 and glass/FTO/PEDOT:PSS at RT. Tick marks indicate the position of allowed reflections in *I*4*cm*. The asterisk indicates the (110) reflection of FTO.

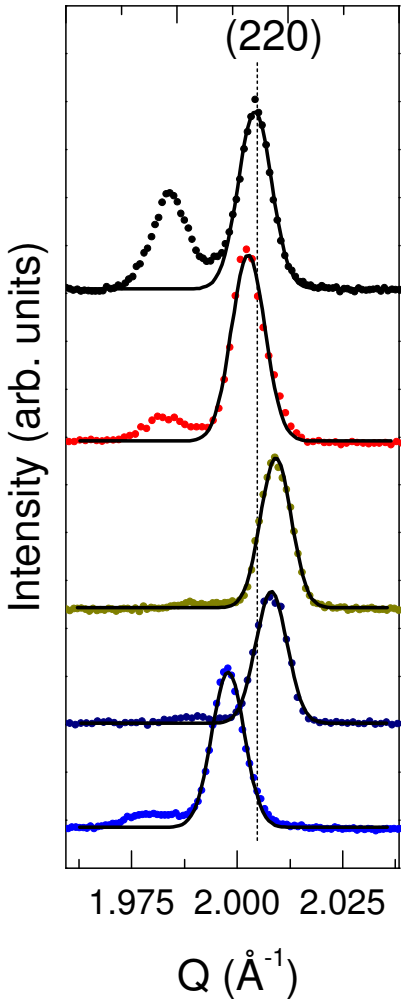

Figure S5.SXRPD (λ = 0.826 Å) data of $MAPbI_3$ on glass (red), glass/FTO (olive), glass/FTO/TiO_2 (dark blue), glass/FTO/PEDOT:PSS (blue) and $MAPbI_3$ powder (black) at RT. Solid black lines indicate the (220) reflection Voigt fit.

The ratio between the integrated intensity of the (220) reflection (Figure S4 and S5) and the total integrated intensity between 14.5 and 19.5° in two-theta (Figure 2 and S4) has been used as figure of merit of the 110 preferred orientation degree using the **equation S1**,

$$\left[1 - \frac{(A_{220}/A_{14.5°-19.5°})_{powder}}{(A_{220}/A_{14.5°-19.5°})_{x}}\right] \times 100$$

where A_{220} is the (220) integrated intensity, $A_{14.5°\text{-}19.5°}$ represents the total integrated intensity between 14.5 and 19.5° in two-theta for $MAPbI_3$ powder and $MAPbI_3$ on *x* substrate (glass, glass/FTO, glass/FTO/TiO_2, and glass/FTO/PEDOT:PSS).

Note: (*hkl*) indicates a lattice plane, [uvw] a lattice direction and <uvw> indicates a family of [uvw] directions, in that way the family of [110] directions is designated as <110>.

Photoluminescence

Prototypical steady PL emission of $MAPI_3$:Cl thin films on the different substrates exciting at 488 nm laser wavelength with very low power (6 µW, 12 W/cm^2) are shown in left panel of Figure S5. Taking into account reported absorption coefficient [3] we can assume the same sample volume evaluated for each thin film as the absorption depth for 488 nm wavelength was calculated to be around 85 nm. The band maximum arises at 775.5, 778, 775 and 778 nm for glass, PEDOT:PSS, FTO and TiO_2 respectively.

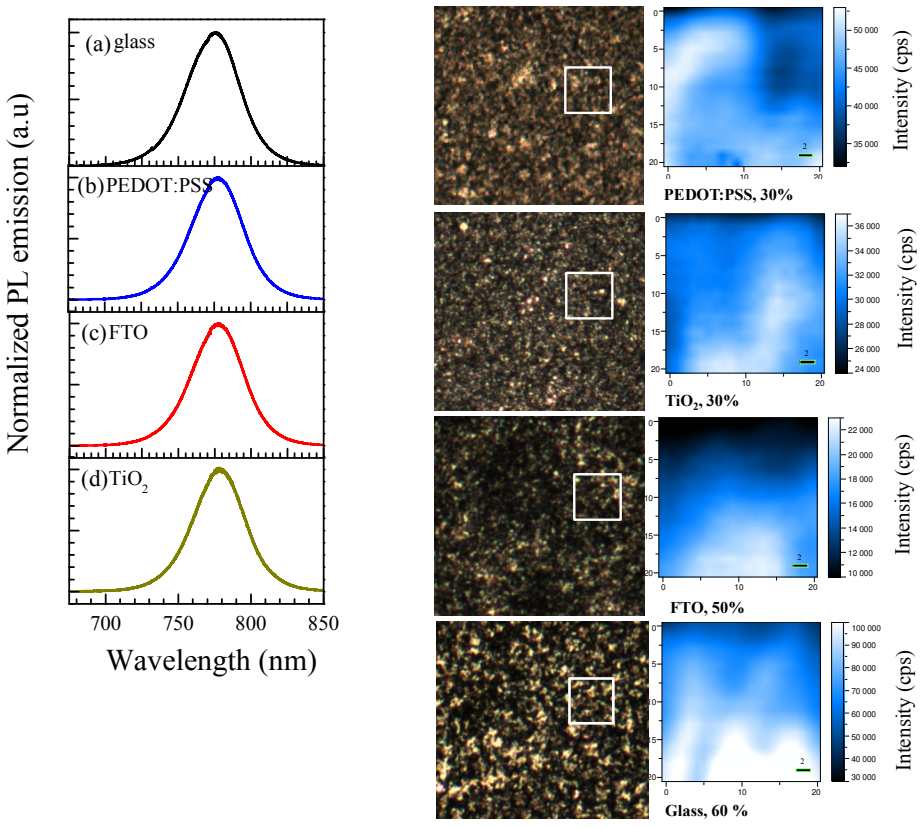

Figure S6. (Left panel) PL emission of the $MAPbI_3$:Cl thin films deposited on glass (a), FTO/pedot:pss (b), FTO (c) and FTO/TiO_2 (d) compact layer. Right panel: variation of the PL intensity in a 20x20 µm area (the white square in the corresponding microphotograph) size, showing % variation between the intensity maximum and minimum.

Raman spectra of the $MAPbI_3$:Cl thin films

In **Table S2** are the measured low frequencies Raman modes (cm^{-1}) at RT with 488 nm excitation of PbI_2, PbO_2 and $MAPbI_3$. Reported PbI_2 and $MAPbI_3$ modes are included for comparison. According to calculations, based on the harmonic approximation and neglecting spin-orbit coupling,[4] the band observed around 120-130 cm^{-1} is due to MA normal modes coupled to some extent to the inorganic cage in the range 140-170 cm^{-1} which are sensitive to the orientation of the MA^+ cation in tetragonal or orthorhombic structures. For the Raman mode at 237 cm^{-1}, the most similar calculated frequencies are torsional modes of the organic cations predicted in the 200−370 cm^{-1} range from more disordered or confined MA to more ordered structure (orthogonal). [4,5,6] It has been reported that the deformation of the MA molecule shifts the torsional mode toward higher frequencies and, on the contrary, the formation of specific hydrogen bonding interactions, typical of these compounds[7,8] shifts this mode toward lower frequencies.

PbI_2 this work	**PbI_2 9**	**PbO_2 This work**	**$MAPbI_3$ theory** 4	**$MAPbI_3$ This work (**)**	**$MAPbI_3$** 4	**$MAPbI_3$ 10**	**$MAPbI_3$ 11**	**$MAPbI_3$:Cl** 6
	72	**83**	72 87		62 94	71 94	52	
115	95,113		141-150	**127(85)**	120	110	110	119
		138			154	140		150-160
210 (*)	214(*)	**278**	200-340	**237(76)**	270	270		250

Table S2. Measured low frequencies Raman modes (cm^{-1}) at RT with 488 nm excitation of PbI_2, PbO_2 and $MAPbI_3$. PbI_2 and $MAPbI_3$ measured and calculated modes reported by different authors are included for comparison. (*) only visible in resonant conditions. (**) In parenthesis the FWHM of the fitted peaks in Figure 3d.

In **Figure S7** we can observe the Raman spectra for increasing incident power laser of $MAPbI_3$:Cl films for the four different substrates in ambient conditions (a-d) at intermediate **stage** and final **stage 5**. We observe different evolution depending of the substrate. The intermediate stage (blue line) corresponds with the situation where PL emission is partially quenched. The bands around 110 cm^{-1} and 165 cm^{-1} are clearly detected and for higher laser power, in the final stage (green lines), the peak associated

to the formation of PbOx around 138-140 cm^{-1} is dominating the spectra except for the case of PEDOT:PSS substrate.

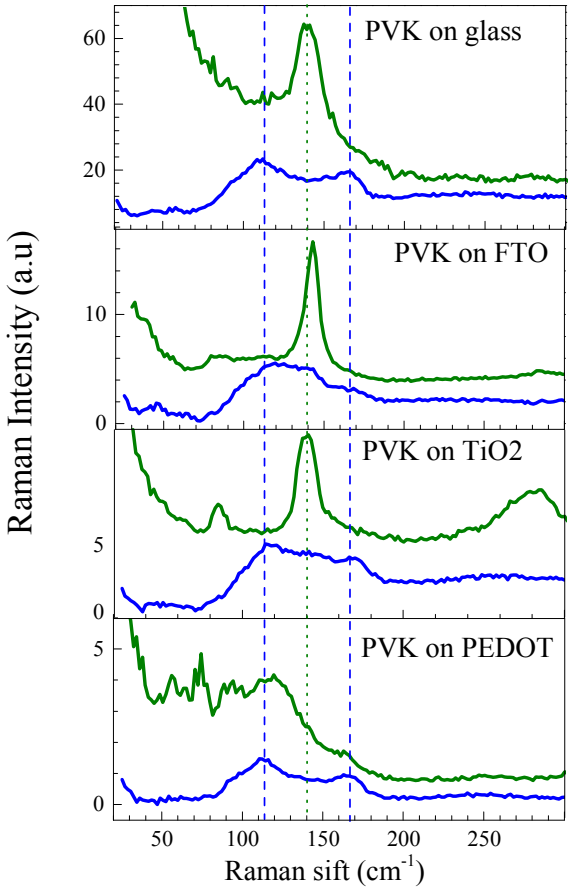

Figure S7. (a-d) Micro Raman spectra for the $MAPbI_3$:Cl thin films for the four substrates at intermediate (blue) and final (green) stages with increasing incident power.

[1] I. Horcas, R. Fernández, JM. Gómez-Rodríguez, J. Colchero, J. Gómez-Herrero, Baro AM. *Rev.Sci.Instrum*. **2007**, 78, 013705.

[2] C. C. Stoumpos, C. D. Malliakas, M. G, Kanatzidis. *Inorg. Chem.* **2013**, *52* (15), 9019–9038.

[3] G. Xing, N. Mathews, S. Sun, S. S. Lim, Y. M. Lam, M. Grätzel, S. Mhaisalkar, T. C. Sum. *Science*.**342**, 344–347 (2013).

[4] C. Quarti, G. Grancini, E. Mosconi, P. Bruno, J. M. Ball, M. M. Lee, H. J. Snaith, A. Petrozza, and F. De Angelis. *J. Phys. Chem. Lett*. **2014**, 5, 279−284.

[5] F. Brivio, J. M. Frost, J. M. Skelton, A. J. Jackson, O. J. Weber, M. T. Weller, A. R. Goni, A. M. A. Leguy, P. R. F. Barnes, and A. Walsh. *Phys. Rev. B*. **2015**, 92, 144308.

[6] G. Grancini, S. Marras, M. Prato, C. Giannini, C. Quarti, F. De Angelis, M. De Bastiani, G. E. Eperon, H. J. Snaith, L. Manna, and A. Petrozza. *J. Phys. Chem. Lett*. **2014**, 5, 3836−3842.

[7] J. Even, L. Pedesseau, J.-M. Jancu, C. J. Katan. *Phys. Chem. Lett*. **2013**, 4, 2999−3005.

[8] D. B. Mitzi. *J. Chem. Soc*., *Dalton Trans*. **2001**, 1−12.

[9] I. Baltog, M. Baibarac, S. Lefrant. *J Phys Condens Matter*. **2009,** Jan 14;21(2):025507.

[10] B.W. Park, S. M. Jain, X. Zhang, A. Hagfeldt, G. Boschloo, and T. Edvinsson. *ACS Nano*. **2015**, 9, 2088.

[11] M. Ledinský,P. Löper, B. Niesen, J. Holovský, S-J. Moon, J.-H. Yum, S. De Wolf, A. Fejfar, and C. Ballif. *J. Phys. Chem. Lett*. **2015**, 6, 401−406.